Available online at www.sciencedirect.com
SCIENCE DIRECT®
Journal of Sound and Vibration 291 (2006) 882–901
JOURNAL OF SOUND AND VIBRATION
www.elsevier.com/locate/jsvi

Sound propagation in an array of narrow porous channels with application to diesel particulate filters

Sabry Allam, Mats Åbom*

The Marcus Wallenberg Laboratory for Sound and Vibration Research, Department of Aeronautical and Vehicle Engineering, KTH, SE-10044 Stockholm, Sweden

Received 14 February 2005; received in revised form 27 May 2005; accepted 4 July 2005
Available online 15 September 2005

Abstract

In an earlier work the authors have presented a 1-D acoustic model for diesel particulate filters (DPFs). One shortcoming of this first model is the approximate treatment of the viscous and thermal losses along the narrow channels. In the present paper this issue is analyzed in more detail, by solving the convective acoustic wave equations for two neighboring channels simplified in the manner of the Zwikker and Kosten theory. From the solution the acoustic two-port has been calculated to predict the sound transmission losses for an entire DPF unit. The theoretical results are compared with experimental data for clean filter units at room temperature and the agreement is very good and better, in particular for very small Mach numbers, than for the earlier presented 1-D model. A modified 1-D model using the classical (exact) Kirchhoff solution for a plane wave in a narrow tube is also presented. This modified 1-D model is in close agreement with the predictions of the new model. Furthermore, the earlier proposed 1-D model, which assumes isothermal sound propagation, works satisfactorily up to 800–1000 Hz for a typical filter at operating (hot) conditions.

1. Introduction

Generally the propagation of acoustic waves in a homogeneous thermo-viscous fluid at rest, unbounded in all directions, involves reactive and dissipative processes that can be characterized,

*Corresponding author. Tel.: +46 8 790 7944; fax: +46 8 790 6122.
E-mail address: matsabom@kth.se (M. Åbom).

0022-460X/$ - see front matter © 2005 Elsevier Ltd. All rights reserved.
doi:10.1016/j.jsv.2005.07.022

in the frequency domain, by a complex-valued wavenumber, the imaginary part of which is proportional to the shear and bulk viscosity coefficients and the heat conduction coefficient. It can also include dissipation processes due to molecular relaxation via a complex-valued specific heat ratio [1]. In a bounded domain (pipe or cavity), reactive and dissipative processes at rigid walls arise from interactions between the acoustic field and the entropy (diffusion of heat) and the vorticity fields (diffusion of shear waves), created on the boundary walls and extracting energy from the acoustic wave. The entropy and vorticity fields decay exponentially in the direction normal to the walls and, with the exception of low frequencies and narrow ducts, only play a role in a thin acoustic boundary layer region. When this is the case the effect of resulting reactive and dissipative effects can still be handled by introducing a complex wavenumber. For the case of interest here with sound propagation in a narrow channel (width around 1 mm) the boundary layers will extend over the cross-section and a full analysis of the coupled field problem is necessary.

The case of sound waves in a visco-thermal fluid inside a cylindrical, rigid and narrow pipe with no flow was solved exactly already by Kirchhoff [2]. During the last decade there has been an interest to extend this solution to other cross-section shapes and to account for the effects of a mean flow. One reason for this interest has been the efforts to model automobile catalytic converters [3–8].

Peat [3] and Astley and Cummings [4] presented FEM solutions, based on simplified equations for waves in a visco-thermal fluid, for the problem of sound propagation in capillary tubes. The analysis is for laminar mean flow with a parabolic velocity distribution and a quadratic cross-section. The simplification of the governing equations is discussed in some detail by Astley and Cummings [4] and is based on the assumption that the axial gradients are much smaller than the gradients over the cross-section. Dokumaci [5] using the same set of simplified equations showed that for the case of a plug flow and a circular cross-section an exact solution is possible. Using this model the acoustic two-port for a catalytic converter unit was derived. Ih et al. [6] have developed analytical solutions for sound propagation in capillary cylindrical tubes with a parabolic mean flow, by neglecting the radial component of the particle velocity. Jeong and Ih [7] showed by numerical solutions of the governing equations, that including the radial particle velocity has a small but noticeable effect. In a later work Dokumaci [8] extended his earlier work [5] to the case of rectangular narrow tubes with a plug flow. The solution procedure is now based on a weak (Galerkin) formulation, where the fields over the channel cross-section are expanded as double Fourier sinus series.

For the case of diesel particulate filters there is a need to analyze wave propagation in narrow tubes (width 1–2 mm) taking into account the effect of wall porosity. All the works discussed above are for the case of tubes with rigid and non-porous walls, and are therefore not applicable. To develop a model for diesel particulate filters the model suggested by Dokumaci [8] will be used and modified to include the effect of wall permeability.

2. Formulation and solution of the problem

With reference to Fig. 1, a DPF unit can be slit into 5 parts: the inlet cross-section (IN), narrow pipes with impermeable walls (I) and (III), the ceramic monolith section (II), and the outlet

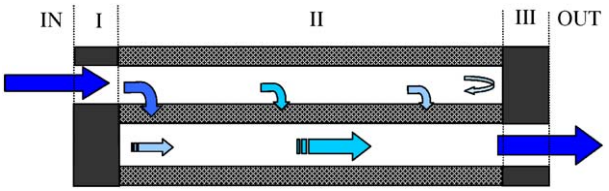

Fig. 1. Cross-section of a unit cell in a DPF split into five sections each described by an acoustic two-port. Note, the filter section (II) is actually an acoustic four-port but can be reduced to a two-port due to the hard walls in sections I and III.

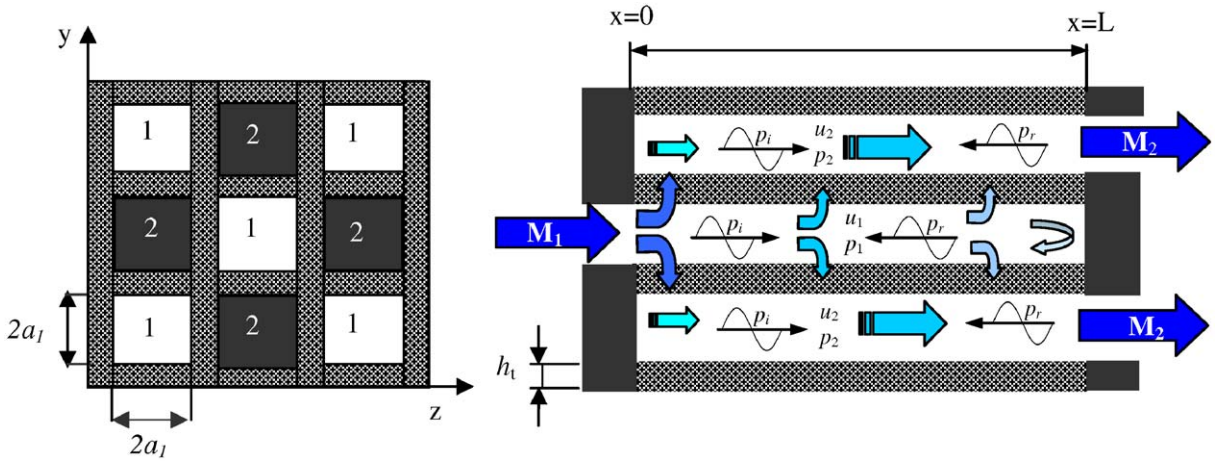

Fig. 2. Neighboring channels in a DPF unit. The flow and the acoustic waves enter the channels (1) open upstream and closed downstream, then pass through the porous walls into the channels (2) closed upstream and open downstream.

cross-section (OUT). In the plane wave range these parts can be described via two-port transfer matrices (**T**). The resulting transfer matrix for a filter unit is then simply

$$\mathbf{T}_{\mathrm{DPF}} = \mathbf{T}_{\mathrm{IN}}\mathbf{T}_{\mathrm{I}}\mathbf{T}_{\mathrm{II}}\mathbf{T}_{\mathrm{III}}\mathbf{T}_{\mathrm{OUT}}. \tag{1}$$

2.1. The governing equations for the filter section (II)

The structure of diesel particulate filter cells is approximately square in the cross-section with a width that (on the inlet side) can vary due to accumulated soot particles. To develop a model for the wave propagation the knowledge of the propagation constant for two neighboring cells in the filter is required; see Fig. 2.

The linearized conservation equations for momentum, mass and energy, simplified in the manner appropriate for narrow pipes, see Ref. [9], are for harmonic time variation [$e^{i\omega t}$]

$$\rho_{0j}\left(\mathrm{i}\omega + U_{0j}\frac{\partial}{\partial x}\right)u_{xj} + \rho_{0j}\frac{\partial U_{0j}}{\partial x}u_{xj} = -\frac{\partial p_j}{\partial x} + \mu_j\nabla_s^2 u_{xj}, \quad p_j = p_j(x,t), \tag{2}$$

$$\left(\mathrm{i}\omega + U_{0j}\frac{\partial}{\partial x}\right)\rho_j + \frac{\partial U_{0\mathrm{j}}}{\partial x}\rho_j + \frac{\partial \rho_{0j}}{\partial x}u_{xj} + \rho_{oj}\nabla\cdot\mathbf{u}_j = 0, \tag{3}$$

$$\rho_{0j}C_{pj}\left(\mathrm{i}\omega + U_{0j}\frac{\partial}{\partial x}\right)T_j + \rho_{0j}C_{pj}\frac{\partial T_{oj}}{\partial x}u_{xj} + U_{0j}C_{pj}\frac{\partial T_{0j}}{\partial x}\rho_j = \left(\mathrm{i}\omega + U_{0j}\frac{\partial}{\partial x}\right)p_j + \frac{\partial P_{oj}}{\partial x}u_{xj} + k_{\mathrm{th}j}\nabla_s^2 T_j, \quad T_j = T_j(x,y,z,t), \tag{4}$$

where an ideal gas is assumed and chemical reactions are neglected. The ideal gas law in linearized form implies

$$\rho_j = \left(\frac{p_j}{R_j T_{0j}}\right) - \left(\frac{\rho_{0j}T_j}{T_{0j}}\right), \quad \rho_j = \rho_j(x,y,z,t). \tag{5}$$

Here, x denotes the channel axis, $\mathbf{u}$ is the acoustic particle velocity, $j = 1,2$ represent the inlet and outlet pipes, respectively, p, T and δ are the acoustic pressure, temperature and density, respectively, μ is the shear viscosity coefficient, k_{th} is the thermal conductivity of the fluid, R is the gas constant, C_p is the specific heat coefficient at constant pressure, P_0, T_0 and ρ_0 denote the ambient pressure, temperature and density, respectively, U_0 denotes the axial mean flow velocity and ∇_s^2 denotes the Laplacian over the channel cross-section. The boundary conditions that must be satisfied by $\mathbf{u}$ and T on the walls are $u_w = \mathbf{u}_1\cdot\mathbf{n}_1 = -\mathbf{u}_2\cdot\mathbf{n}_2$ and $T = 0$, where $\mathbf{n}$ is the outward normal vector for the channel wall. It is assumed here that the introduced non-zero normal velocity at the walls is very small compared to the axial fluctuating velocity, so that the simplifying assumptions in the model [9] are still valid. This issue will be checked later when calculations for actual filters are presented.

To describe the coupling between neighboring channels Darcy's law is applied to the fluctuating fields [10]

$$p_1 - p_2 = R_w u_w, \tag{6}$$

where u_w is the acoustic velocity through the wall and R_w is the wall resistance, which is given by $R_w = \mu_w h_t/\sigma_w$, where μ_w is the dynamic viscosity, h_t the wall thickness and σ_w the wall permeability.

2.2. Calculation of propagation constants and two-port matrix

To solve the problem a segmentation approach will be applied. This means that the filter section is split into a number of elements in series and in each element the mean flow state and gradients of the mean flow state are assumed to be constant. The solution for this segmented filter will approach the correct solution when the number of segments goes to infinity. In practice the number of segments needed to achieve a certain accuracy depends on the magnitude of the gradients, see Section 2.6.

To solve the equations in each segment the fields are assumed [8] to have the following form:

$$p_j = A_j\exp(-\mathrm{i}\Gamma k_1 x), \quad u_{xj} = H_j(y,z)p_j, \quad T_j = F_j(y,z)p_j, \tag{7}$$

where A_j is an arbitrary constant, $k = \omega/c$ is the wave number, Γ is the propagation constant and $0 \le y \le 2a_j$, $0 \le z \le 2a_j$. Substituting Eq. (7) into Eq. (2), dropping p_j from both sides of the

equation and rearranging yields

$$\frac{\partial^2 H_j}{\partial y^2}+\frac{\partial^2 H_j}{\partial z^2}-\beta_j^2 H_j=\frac{-\mathrm{i}\Gamma k_1}{\mu_j} \tag{8}$$

with

$$\beta_j^2=\mathrm{i}\left(1-\Gamma M_j+\frac{1}{\mathrm{i}\omega}\frac{\partial U_{0j}}{\partial x}\right)s_j^2. \tag{9}$$

Here $s_j=\sqrt{\rho_{0j}\omega/\mu_j}$, $M_j=U_{0j}/c_1$ is the mean flow Mach number and s is a shear wavenumber.

By using the ideal gas state Eqs. (5), (7) and (9) in the energy Eq. (4) and dropping p_j yields

$$\frac{\partial^2 F_j}{\partial y^2}+\frac{\partial^2 F_j}{\partial z^2}-\sigma_j^2 F_j=\sigma_{0j}^2+\sigma_{1j}^2 H_j, \tag{10}$$

where

$$\sigma_j^2=\mathrm{i}\xi_j^2 s_j^2\left(1-\Gamma M_j-\frac{U_{0j}}{\mathrm{i}\omega T_{0j}}\frac{\partial T_{0j}}{\partial x}\right),\quad \xi_j^2=\left(\frac{\mu_j C_{pj}}{k_{\mathrm{th}j}}\right),\ \text{the Prandtl number},$$
$$\sigma_{0j}^2=\frac{-\mathrm{i}\omega\left(1-\Gamma M_j-\dfrac{C_{pj}U_{0j}}{\mathrm{i}\omega R_j T_{0j}}\dfrac{\partial T_{oj}}{\partial x}\right)}{k_{\mathrm{th}j}}\quad\text{and}\quad \sigma_{1j}^2=\frac{1}{k_{\mathrm{th}j}}\left(\rho_{0j}C_{pj}\frac{\partial T_{0j}}{\partial x}-\frac{\partial P_{0j}}{\partial x}\right). \tag{11}$$

In order to find a solution to Eq. (8) in a weak (Galerkin) sense the field is expanded in a double Fourier sinus series

$$H_j(y,z)=\sum_{m,n}a_{mn}\sin\left(\frac{m\pi y}{2a_j}\right)sin\left(\frac{n\pi z}{2a_j}\right),\quad m,n=1,3,5,7,\ldots. \tag{12}$$

This series only includes symmetric terms since the assumed pressure distribution is symmetric over the cross-section (a constant) and the no slip wall boundary condition is satisfied by all the terms. The coefficients a_{mn} are determined by substituting the series into Eq. (8), integrating the result over the pipe cross-section and using the orthogonality property of the terms (see Appendix A). The result is

$$a_{mn}=\frac{16\mathrm{i}k_1\Gamma}{\pi^2 mn\,\mu_j\beta_j^2\alpha_{mn}(\beta_j a_j)}, \tag{13}$$

where $\alpha_{mn}(\beta_j a_j)=(1+\pi^2/4(\beta_j a_j)^2(m^2+n^2))$.

The same method can be applied to Eq. (10), i.e., F_j can also be expressed in the form of a double Fourier sinus series

$$F(y,z)=\sum_{m,n}b_{mn}\sin\left(\frac{m\pi y}{2a_j}\right)\sin\left(\frac{n\pi z}{2a_j}\right),\quad m,n=1,3,5,7,\ldots, \tag{14}$$

where the coefficients b_{mn} are found analogous to the case already treated and are given by

$$b_{mn} = -\frac{1}{\sigma_j^2 \alpha_{mn}(\sigma_j a_j)}\left(\frac{16\sigma_{0j}^2}{\pi^2 mn} + \sigma_{1j}^2 a_{mn}\right). \tag{15}$$

In order to close the problem the mass conservation equation (3) is now used to obtain an eigenvalue equation for the unknown wavenumber. Averaging Eq. (3) over the channel cross-section yields

$$\left(i\omega + U_{0j}\frac{\partial}{\partial x}\right)\langle \rho_j \rangle + \frac{\partial U_{0j}}{\partial x}\langle \rho_j \rangle + \frac{\partial \rho_{0j}}{\partial x}\langle u_{xj} \rangle + \rho_{0j}\langle \nabla \cdot u_j \rangle = 0, \tag{16}$$

where $\langle f \rangle = (1/4a_j^2)\iint_{2a_j x 2a_j} f \, \mathrm{d}y \, \mathrm{d}z$. The first and the second term in Eq. (16) can be rewritten using the linearized ideal gas law equations (5) and (7) as

$$\langle \rho_j \rangle = \frac{\langle p_j \rangle}{R_j T_{0j}} - \frac{\rho_{0j}\langle T_j \rangle}{T_{0j}} = \frac{p_j}{R_j T_{0j}}\left(1 - \rho_{0j} R_j \langle F_j \rangle\right). \tag{17}$$

The average of the function F_j over the channel cross-section can be calculated using Eqs. (14) and (15). The result is

$$\langle F_j \rangle = \sum_{m,n} \frac{4 b_{mn}}{mn\pi^2}. \tag{18}$$

The third term in Eq. (16) can be rewritten using Eq. (7) as

$$\langle u_{xj} \rangle = p_j \langle H_j \rangle, \tag{19}$$

where the average of H_j is obtained from Eqs. (12) and (13)

$$\langle H_j \rangle = \sum_{m,n} \frac{4 a_{mn}}{mn\pi^2}. \tag{20}$$

The last term in Eq. (16) can be rewritten using the 2-D version of Gauss formula as

$$\langle \nabla \cdot \mathbf{u}_j \rangle = \frac{1}{4a_j^2}\iint_{2a_j x 2a_j}\left(\frac{\partial u_{xj}}{\partial x} + \nabla_s \cdot \mathbf{u}_j\right) d\, y \, \mathrm{d}z = \frac{\partial \langle u_{xj} \rangle}{\partial x} + \frac{1}{4a_j^2}\oint_{C_j} \mathbf{u}_j \cdot \mathbf{n}_j \, \mathrm{d}s, \tag{21}$$

where C_j denotes the curve around the channel perimeter. Introducing the acoustic wall velocity u_w in the last term gives

$$\oint_{C_j} \mathbf{u}_j \cdot \mathbf{n}_j \, \mathrm{d}s = (-1)^{j-1}\oint_{C_j} u_w \, \mathrm{d}s = (-1)^{j-1} 8 a_j \bar{u}_w \tag{22}$$

where the overbar denotes an average along the perimeter. This, by using Darcy's law equation (6), can be written as

$$\oint_{C_j} \mathbf{u}_j \cdot \mathbf{n}_j \, \mathrm{d}s = (-1)^{j-1}\frac{8 a_j (p_1 - p_2)}{R_w}, \tag{23}$$

where the overbar has been dropped since the acoustic pressure is constant over the cross-section. Inserting the pressure field from Eq. (7) in the first term of Eq. (21) gives

$$\frac{\partial\langle u_{xj}\rangle}{\partial x} = \langle H_j\rangle \frac{\partial p_j}{\partial x} = -\mathrm{i}\Gamma k_1 \langle H_j\rangle p_j. \tag{24}$$

Using Eqs. (17)–(24) and the expression for the pressure field, Eq. (16) can be rewritten as

$$\left[\frac{1}{R_j T_{0j}}\left(\mathrm{i}\omega - \mathrm{i}\Gamma k_1 U_{0j} + \frac{\partial U_{0j}}{\partial x}\right)\left(1 - \rho_{0j} R_j \langle F_j\rangle\right) + \left(\frac{\partial \rho_{oj}}{\partial x} - \mathrm{i}\Gamma k_1 \rho_{0j}\right)\langle H_j\rangle\right] A_j + (-1)^{j-1}\frac{2\rho_{0j}(A_1 - A_2)}{a_j R_w} = 0. \tag{25}$$

Eq. (25) represents a homogenous linear equation system for the amplitudes of the pressure waves (A_1, A_2) in channels 1 and 2, which can be written as

$$\begin{bmatrix} K_{11} + K_{21} & -K_{21} \\ K_{22} & K_{12} - K_{22} \end{bmatrix}\begin{pmatrix} A_1 \\ A_2 \end{pmatrix} = \begin{pmatrix} 0 \\ 0 \end{pmatrix}, \tag{26}$$

where

$$K_{1j} = \left[\frac{R_w a_j}{2\rho_{0j} R_j T_{0j}}\left(\mathrm{i}\omega - \mathrm{i}\Gamma k_1 U_{0j} + \frac{\partial U_{0j}}{\partial x}\right)\left(1 - \rho_{0j} R_j \langle F_j\rangle\right) + \frac{R_w a_j}{2\rho_{0j}}\left(\frac{\partial \rho_{0j}}{\partial x} - \mathrm{i}\Gamma k_1 \rho_{0j}\right)\langle H_j\rangle\right]$$

and $K_{2j} = (-1)^{j-1}$.

For non-trivial solutions the determinant should be equal to zero. This leads to a transcendental equation for the propagation constant Γ that can be solved by iteration using the Newton–Raphson method. As discussed by Dokumaci [8], within the simplifications used in the present theory, only the least attenuated (plane wave type) of acoustic mode will emerge. This implies that the eigenvalue problem here, precisely as the 1-D model presented earlier [11], will produce four roots. Since the Mach number in typical filters is very small (<0.1), the no-flow values for the roots given in Ref. [11] can be used to obtain starting values for the iteration. The resulting propagation constants for a typical filter are shown in Fig. 3 assuming no mean flow. Note that for this case the roots corresponding to propagation in the positive or negative x direction differ simply by a minus. The roots in Fig. 3 can be grouped in two categories. One category is the two roots corresponding to uncoupled waves that are identical to the roots obtained by Dokumaci [8]. The other category is two new roots corresponding to coupled waves that are significantly more damped than the uncoupled waves (Fig. 4).

To each of the roots or eigenvalues there is a corresponding 2-D mode (eigenvector) $\mathbf{e}_n$. Using these eigenvalues and modes, a general expression for the sound field in the filter section can be written as

$$\begin{pmatrix} \hat{p}_1(x) \\ \hat{p}_2(x) \end{pmatrix} = \sum_{n=1}^{4} \hat{a}_n \mathrm{e}^{-\mathrm{i}k_1\Gamma_n x}\mathbf{e}_n, \tag{27}$$

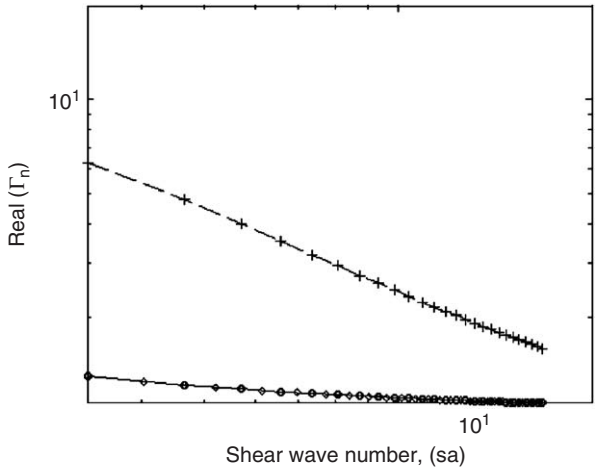

Fig. 3. Real part of the propagation constants versus normalized shear wavenumber (*sa*) for a typical DPF. No flow is assumed and the filter data are taken from Table 1 and $T_0 = 293\,\mathrm{K}$. $^{\circ\circ\circ}$, Γ_1; —, $-\Gamma_2$ propagation constants for uncoupled waves and $\diamond\diamond\diamond$, propagation constant for Dokumaci [8]. $+++$, Γ_3 and ----, $-\Gamma_4$ propagation constants for coupled waves.

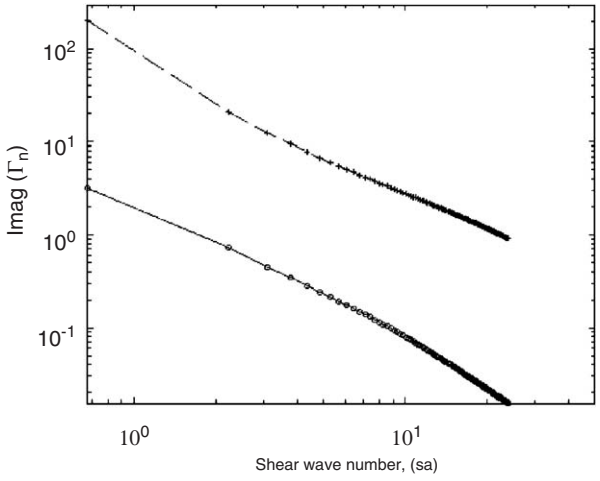

Fig. 4. Imaginary part of the propagation constants ($-\Gamma$) versus normalized shear wave number (*sa*) for a typical DPF. No flow is assumed and the filter data are taken from Table 1 at $T_0 = 293\,\mathrm{K}$. $^{\circ\circ\circ}$, Γ_1; —, $-\Gamma_2$ propagation constants for uncoupled waves and $\diamond\diamond\diamond$, propagation constant for Dokumaci [8]. $+++$, Γ_3 and ----, $-\Gamma_4$ propagation constants for coupled waves.

where $\hat{a}_n$ are the modal amplitudes. From this equation the acoustic volume flows can be obtained using Eq. (7) after integration over the channel cross-sectional area

$$\begin{pmatrix} \hat{q}_1(x) \\ \hat{q}_2(x) \end{pmatrix} = \sum_{n=1}^{4} \hat{a}_n \mathrm{e}^{-ik_1\Gamma_n x} \mathbf{e}'_n, \tag{28}$$

where $e'_{j,n} = 4a_j^2 \langle H_{j,n} \rangle e_{j,n}$. Eqs. (27) and (28) will now be used to obtain the acoustic four-port in transfer matrix form for the filter section. First the following relationship between p and q and modal amplitudes can be written down:

$$\begin{pmatrix} \hat{p}_1(x) \\ \hat{p}_2(x) \\ \hat{q}_1(x) \\ \hat{q}_2(x) \end{pmatrix} = \begin{pmatrix} \mathrm{e}^{-\mathrm{i}k_1\Gamma_1 x}\mathbf{e}_1 & \mathrm{e}^{-\mathrm{i}k_1\Gamma_2 x}\mathbf{e}_2 & \mathrm{e}^{-\mathrm{i}k_1\Gamma_3 x}\mathbf{e}_3 & \mathrm{e}^{-\mathrm{i}k_1\Gamma_4 x}\mathbf{e}_4 \\ \mathrm{e}^{-\mathrm{i}k_1\Gamma_1 x}\mathbf{e}'_1 & \mathrm{e}^{-\mathrm{i}k_1\Gamma_2 x}\mathbf{e}'_2 & \mathrm{e}^{-\mathrm{i}k_1\Gamma_3 x}\mathbf{e}'_3 & \mathrm{e}^{-\mathrm{i}k_1\Gamma_4 x}\mathbf{e}'_4 \end{pmatrix} \begin{pmatrix} \hat{a}_1 \\ \hat{a}_2 \\ \hat{a}_3 \\ \hat{a}_4 \end{pmatrix}. \tag{29}$$

Introducing the notation $\mathbf{H}(x)$ for the matrix in Eq. (29) the four-port matrix $\mathbf{S}$ for the filter section, extending from $x = 0$ to $x = L$, is given by [11]

$$\mathbf{S} = \mathbf{H}(0)\mathbf{H}^{-1}(L). \tag{30}$$

The four-port matrix $\mathbf{S}$ can be used in a two-port matrix $\mathbf{T}$ by using the rigid wall boundary conditions in channels 1 and 2, i.e., $\hat{q}_2(0) = 0$ and $\hat{q}_1(L) = 0$. A straightforward derivation reveals that

$$\begin{pmatrix} \hat{p}_1(0) \\ \hat{q}_1(0) \end{pmatrix} = \mathbf{T} \begin{pmatrix} \hat{p}_2(L) \\ \hat{q}_2(L) \end{pmatrix}, \quad \text{with} \quad \mathbf{T} = \begin{pmatrix} S_{12} - S_{42}S_{11}/S_{41} & S_{14} - S_{44}S_{11}/S_{41} \\ S_{32} - S_{42}S_{31}/S_{41} & S_{34} - S_{44}S_{31}/S_{41} \end{pmatrix}. \tag{31}$$

To obtain the total acoustic volume flow all the open channels (N) at the inlet ($x = 0$) and the outlet ($x = L$) should be added. This implies that the two-port matrix $\mathbf{T}_{\mathrm{II}}$ for the entire filter section (including all channels) is related to the $\mathbf{T}$-matrix in Eq. (31) via

$$\mathbf{T}_{\mathrm{II}} = \begin{pmatrix} T_{11} & T_{12}/N \\ NT_{21} & T_{22} \end{pmatrix}. \tag{32}$$

2.3. Limitations of the model

There are two limitations that need to be addressed. The first limitation concerns the assumption that axial gradients are smaller than gradients over the channel cross-section. This assumption, which is the basis for deducing the simplified set of governing equations used [9], is not valid at the channel openings or at the blocked end of the channels. At these locations there exist "near fields" that are not included in the present analysis. As will be validated later by the good agreement with experiments, the effect of these "near fields" is assumed to be negligible. The second limitation concerns the wall permeability, which must be sufficiently small for the assumption of constant pressure over the channel cross-section to be valid. For the acoustic field this assumption is valid as long as the wall impedance $\left(R_w = \mu_w h_t/\sigma_w\right)$ is much higher than the characteristic plane wave impedance ($\rho_{0j}c_j$). For typical filters the ratio between these impedances is of the order of 100 at 20 °C and will increase with increasing temperature.

2.4. Modified version of the 1-D model [11]

In Ref. [11] a 1-D model based on the assumption of isothermal wave propagation in the narrow channels was presented. It is possible to modify this model by using a more general model

for the wave propagation. One possibility is to assume a plane thermo-viscous wave field with characteristics defined by the Kirchhoff solution for a cylindrical pipe [12]. This Kirchhoff version of the 1-D model is obtained by dropping the viscous friction factor α_j and substituting the following values for the speed of sound (c_j) and density (ρ_{0j}), in the equations in Ref. [11].

$$\rho_j = \frac{\rho_{0j}}{\left(1 - F(s_j)\right)},$$
$$c_j = c_{0j}^{\mathrm{ad}} \frac{\left(1 - F(s_j)\right)^{1/2}}{\left[1 + (\gamma - 1)F(\xi_j s_j)\right]^{1/2}}. \tag{33}$$

here c_{0j}^{ad} is the adiabatic speed of sound in channel no. j and

$$F(s) = \frac{2}{s\sqrt{-\mathrm{i}}} \frac{J_1(\sqrt{-\mathrm{i}}s)}{J_0(\sqrt{-\mathrm{i}}s)}, \tag{34}$$

where J is the Bessel function of the first type. To obtain an equivalent radius for the Kirchhoff model the hydraulic radius ($= a_j$) has been used. A comparison between this more general 1-D model and the model proposed above is presented later in this paper.

2.5. The complete filter model

With reference to Fig. 1 and Eq. (1) two-port models are also needed for the in and outlet sections as well as the short straight pipe sections (I and III). Concerning the straight pipe sections these can be modeled using the Dokumaci model for sound in narrow pipes [8]. However, since the length of sections I and III is small (less than 10 mm), it is possible to simply add these pipe sections as an end correction (mass plug) to the in- and outlet sections. The in- and outlet sections represent an area constriction and expansion, respectively, where both acoustic and flow near fields can influence the plane wave transmission. As suggested in Ref. [11] a lumped impedance model can be used for the in- and outlet sections including the adjacent short pipes. This implies that

$$\mathbf{T}_X = \begin{pmatrix} 1 & Z_X \\ 0 & 1 \end{pmatrix}, \tag{35}$$

where $X = \mathrm{IN} + \mathrm{I}$ or $\mathrm{III} + \mathrm{OUT}$, $Z_X = r_X + \mathrm{i}Y_X$ and expressions for the lumped impedance are found in Ref. [11]. There are alternative ways of formulating the acoustic coupling conditions at the IN and OUT sections. One way is to assume conservation of energy at the inlet and conservation of momentum at the outlet where there is flow separation [13–15]. For the case of small Mach numbers these assumptions lead to a two-port with the same structure as in Eq. (35), see Appendix B, with

$$Z_X = \begin{cases} Z_{\mathrm{IN}} M_{\mathrm{IN}}\left(1/m_{\mathrm{IN}}^2 - 1\right) + \mathrm{i}Y_{\mathrm{I}}, \\ 2Z_{\mathrm{OUT}} M_{\mathrm{OUT}}\left(1 - 1/m_{\mathrm{OUT}}\right) + \mathrm{i}Y_{\mathrm{III}}, \end{cases} \tag{36}$$

where $Z_{\mathrm{IN}} = \rho_{\mathrm{IN}} c_{\mathrm{IN}}/A_{\mathrm{IN}}$, $Z_{\mathrm{OUT}} = \rho_{\mathrm{OUT}} c_{\mathrm{OUT}}/A_{\mathrm{OUT}}$, m_{IN} and m_{OUT} are the open area ratios at the inlet and outlet, respectively, and Y_{I} and Y_{III} are the mass plug impedances.

To check the effect of choosing different models for the in- and outlet sections the two models above have been compared; see Section 3.1.

Once all the matrices are determined for a filter unit the total two-port is calculated from Eq. (5). The filter transmission losses can then be obtained from [13]

$$\mathrm{TL} = 10\log_{10}\left\{\left(\frac{1+M_{\mathrm{IN}}}{1+M_{\mathrm{OUT}}}\right)^2 \frac{Z_{\mathrm{IN}}}{4Z_{\mathrm{OUT}}}\left|T_{11}+\frac{T_{12}}{Z_{\mathrm{OUT}}}+Z_{\mathrm{IN}}T_{21}+\frac{Z_{\mathrm{IN}}T_{22}}{Z_{\mathrm{OUT}}}\right|^2\right\}, \tag{37}$$

where M_{IN}, M_{OUT} and Z_{IN}, Z_{OUT} are the Mach numbers and the acoustic wave impedances at the in- and outlet of the filter.

2.6. Temperature and mean-flow gradients

For application to real cases it is necessary to include the effects of temperature and mean-flow gradients. This can be done by splitting the filter section into cells with piecewise constant mean-flow state and mean-flow gradients to approximate the continous variation. The length of each constant state cell is chosen so that it is much shorter than a typical axial length scale for the gradients. For each cell the four-pole matrix is calculated using the theory presented above. The four-pole matrices for all cells are then multiplied to obtain the matrix for the entire filter section. This is then reduced to a two-port as described above. This procedure has been applied to typical DPF units using realistic data for the mean-flow state. The result is that the effect of the gradients is very small and neglecting the gradients and using the average state for the calculations gives, e.g., an error of the order of 0.3 dB for the filter damping. Therefore, in all the calculations presented below the average mean flow state has been used and the gradient terms have been neglected. As shown by the results in Ref. [11] the main effect of flow is related to the inlet and outlet area discontinuity. For practical cases it is actually possible to also neglect mean flow all together when modelling the filter section.

3. Predicted damping for a DPF at operating conditions

To investigate the predictions resulting from the new model and compare with the previous 1-D model [11] a typical DPF will be analyzed. The data used for the calculations are summarized in Table 1 and are identical to the case studied in Ref. [11].

For the fluid state of the unit the following data are assumed: static pressure 1.0E5 Pa, average temperature 775 °K and Mach number 0.020 before the inlet of the DPF. Calculated mean flow and temperature distributions in the DPF have been presented in Ref. [11]. From these results the

Table 1
Data for the studied DPF

Diameter/length (mm)	$n \times 10^{-5}$ (channels/m^2)	Channel width $d_h \times 10^3$ (m)	Wall thickness $h_t \times 10^4$ (m)	Wall permeability $\sigma_w \times 10^{13}$ [m^2]
150/250	3.10	1.44	3.55	2.50

input data needed to calculate the results presented below, i.e., the in- and outlet density and flow speed, can be obtained.

3.1. Acoustic coupling at the in- and outlet

The effect of using two different coupling conditions has been investigated using the model presented above. The first is to use the energy losses due to pressure drop and the second is to use the conservation of energy at the inlet and the conservation of momentum at the outlet with the conservation of mass, to calculate the acoustic two-port in Eq. (35).

As shown in Fig. 5, the difference between the two coupling conditions is small (in the order of 0.15 dB), but physically the second is more correct and in line with earlier published models [14,15].

3.2. Predicted damping

The results for a clean filter and a filter without soot loading are shown in Fig. 6. Concerning the soot loading, a thickness of 1/10 tenth of the wall thickness is assumed and a permeability (σ_{soot}) of 1.5×10^{-14}. The resulting wall resistance with soot loading added is given by

$$R_w = \mu_w \left(\frac{h_t}{\sigma_w} + \frac{h_{\text{soot}}}{\sigma_{\text{soot}}} \right). \tag{38}$$

By substituting this value for the wall resistance into Eq. (6) the theory is modified to include the effect of soot loading.

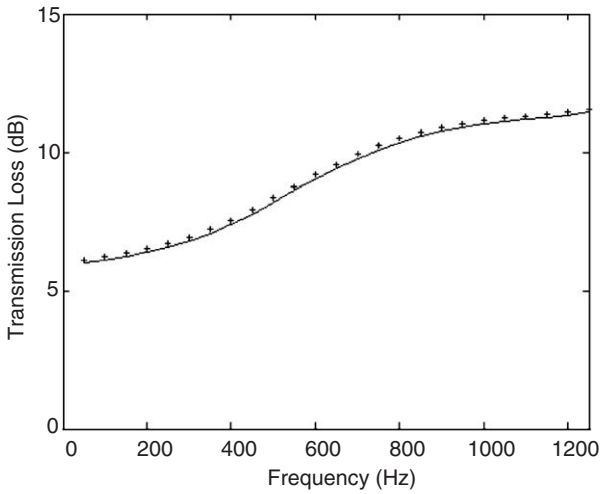

Fig. 5. Transmission loss versus frequency at $M = 0.02$ before the inlet of the DPF and $T_{\text{av}} = 775\,^{\circ}\text{K}$. Effect of different acoustic coupling conditions at the inlet and outlet: + + +, with energy losses on both sides; —, with the conservation of energy at the inlet and conservation of momentum at the outlet.

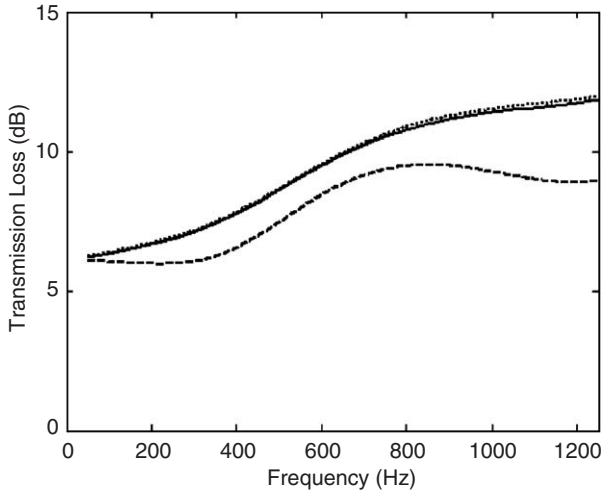

Fig. 6. Predicted transmission loss for the studied filter unit with no soot layer at $T_{av} = 775\,^{\circ}$K. ---, Using the 1-D model [11] and isothermal speed of sound; ……, using the modified 1-D model; —, using the present theory. $M = 0.02$ before the inlet of the DPF.

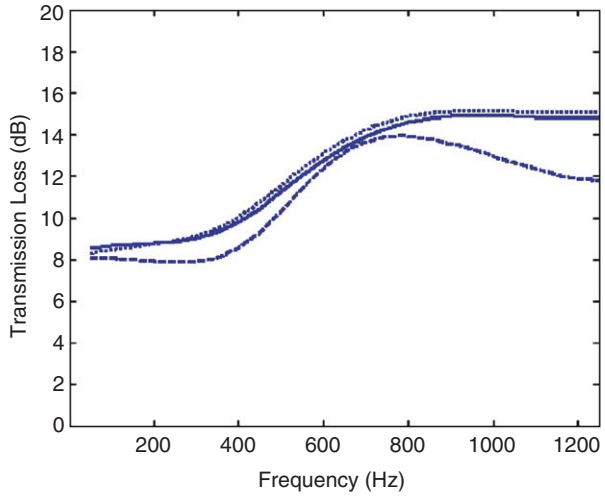

Fig. 7. Predicted transmission loss for the studied filter unit with soot layer at $T_{av} = 775\,^{\circ}$K. ---, Using the 1-D model [11] and isothermal speed of sound; ……, using the modified 1-D model; —, using the present theory. $M = 0.02$ before the inlet of the DPF.

Fig. 6 shows that (i) all models approach the same low-frequency limit, (ii) the simple 1-D model [11] (assuming an isothermal speed of sound) works satisfactorily up to 600–800 Hz and; (iii) the modified 1-D model (see Section 2.4) is in close agreement with the new model presented here. Fig. 7 shows that (i) the damping is strongly affected by soot, which of course is related to the pressure drop increase due to the soot layer; (ii) the simple 1-D model with the isothermal speed of sound now works satisfactorily up to 1000 Hz.

4. Experimental validation at cold conditions

The acoustic two-ports have been measured for four different clean DPF filter units at room temperature (20 °C), which here will be referred to as the "cold" condition. Details of the acoustic test rig and procedure are presented in Ref. [11]. The layout of the test rig is shown in Fig. 8.

The four tested filters all had length of 250 mm and the codes following, RC: (200/12), RC: (200/20), EX80: (100/17) and EX80: (200/14), where (x/y) stands for the number of cells per square inch/wall thickness in inch multiplied by 1000. A summary of the data for the filters is presented in Table 2.

From the discussion in Ref. [11] for the cold case (20 °C), it can be concluded that the quadratic pressure drop (R_2) is dominated by a turbulent channel flow that occurs in a section of the inlet/outlet channels. Assuming that these sections are much shorter than the wavelength, the acoustic effect can be modeled as a lumped resistance at the filter inlet or outlet. The two-port is then

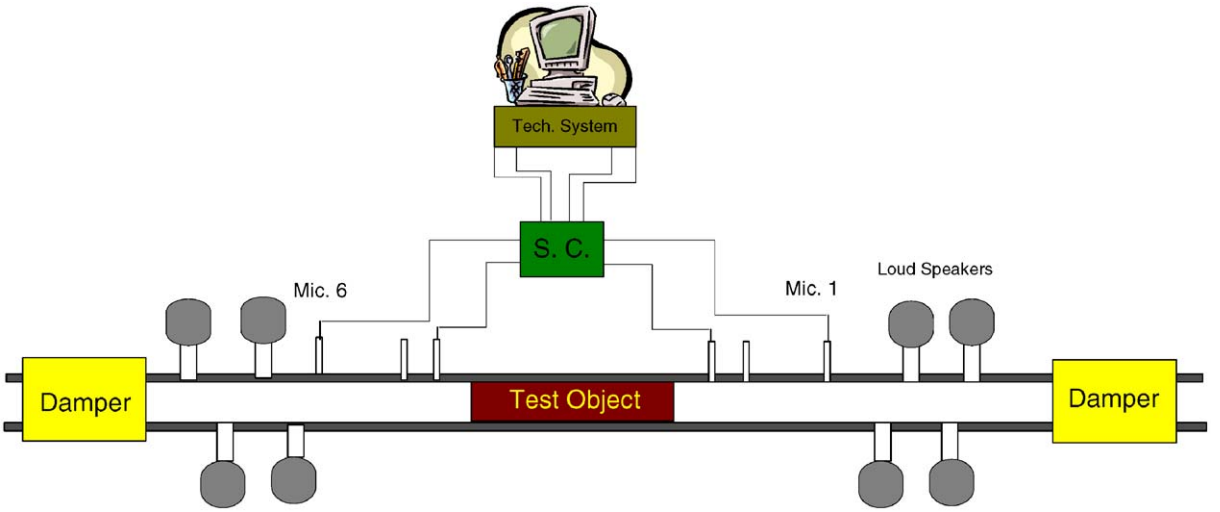

Fig. 8. Layout of the MWL test rig for determination of acoustic two-port data.

Table 2
Data for the tested DPF units including the linear (R_1) and quadratic (R_2) pressure drop (ΔP) coefficients (at 20 °C) determined from measurements: $\Delta P = R_1 U + R_2 U^2$

Filter name	Channel width $d_h \times 10^3$ (m)	Wall thickness $h_t \times 10^4$ (m)	Permeability $\sigma_w \times 10^{13}$ [m^2]	$n \times 10^{-5}$ (channels/m^2)	R_1 (Ns/m^3)	R_2 (Ns^2/m^4)
RC: 200/12	1.5	3.04	25	3.87	87.1	29.2
RC: 200/20	1.3	5.08	25	2.48	233.3	41.56
EX80: 100/17	2.11	4.3	2.5	1.55	199.8	30.92
EX80: 200/14	1.44	3.55	2.5	3.10	184.1	39.2

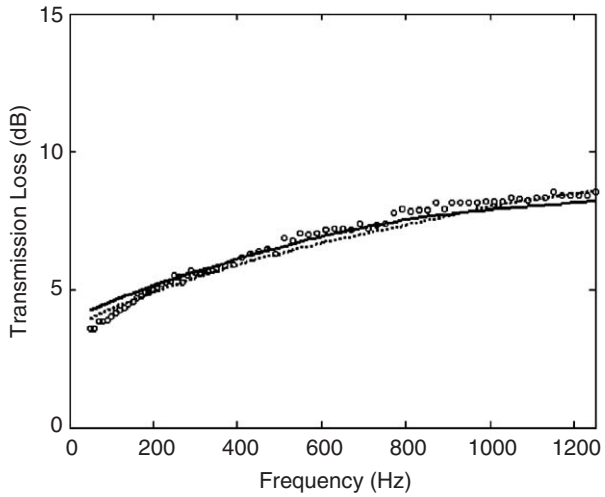

Fig. 9. Measured and predicted transmission loss for the (EX200/14) filter at $M = 0.01$ before the inlet of the DPF unit and $T = 293\,^{\circ}\mathrm{K}$. °°°°, Measured; —, predicted using present theory; …., predicted using the modified 1-D Model.

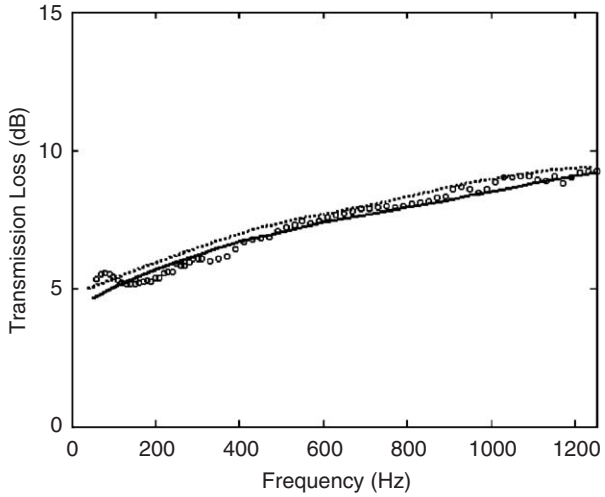

Fig. 10. Measured and predicted transmission loss for the (EX200/14) filter at $M = 0.02$ before the inlet of the filter and $T = 293\,^{\circ}\mathrm{K}$. °°°°, Measured; —, predicted using present theory; …., predicted using the modified 1-D Model.

obtained from Eqs. (35) and (36) with $r_{\mathrm{I+IN}} = r_{\mathrm{III+OUT}} = R_2 U/A$, where U is the flow speed in the main duct and A is the cross-sectional area for the filter. In this equation the losses have been equally split between the inlet and the outlet.

From the measured two-port data the transmission loss has been calculated and compared with the predictions of the proposed models. Examples of modeled and measured transmission loss for the investigated filters are shown in Figs. 9–14. As can be seen from the figures, the new model presented here had a very good agreement with the measured data. The modified 1-D model,

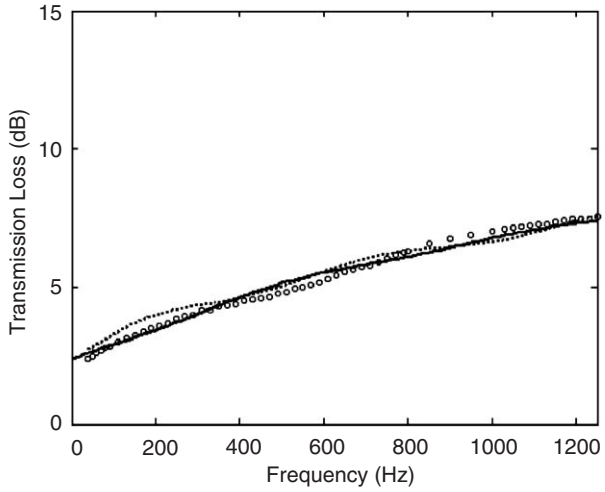

Fig. 11. Measured and predicted transmission loss for the (EX100/17) filter at $M = 0.00$ and $T = 293\,^{\circ}\mathrm{K}$. °°°°, Measured; —, predicted using present theory; …., predicted using the modified 1-D Model.

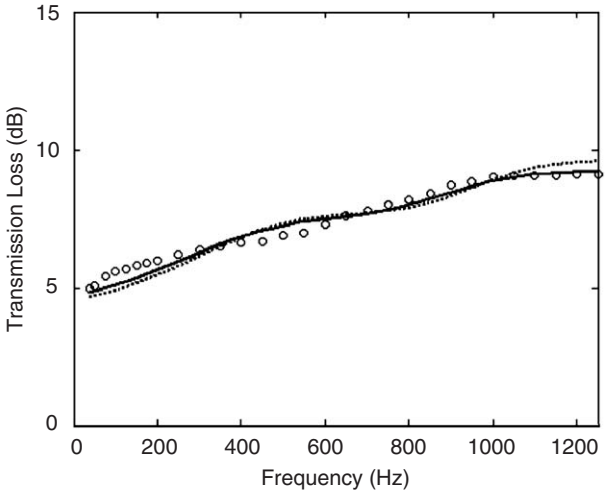

Fig. 12. Measured and predicted transmission loss for the (EX100/17) filter at $M = 0.020$ before the inlet of the filter and $T = 293\,^{\circ}\mathrm{K}$. °°°°, Measured; —, predicted using present theory; …., predicted using the modified 1-D Model.

using wave characteristics obtained from the Kirchhoff solution (Section 2.4), is in close agreement with the new model.

5. Conclusions and future work

A new model for calculation of the acoustic two-port for diesel particulate filters has been presented. Compared to the 1-D model presented earlier [11] this new model includes a correct

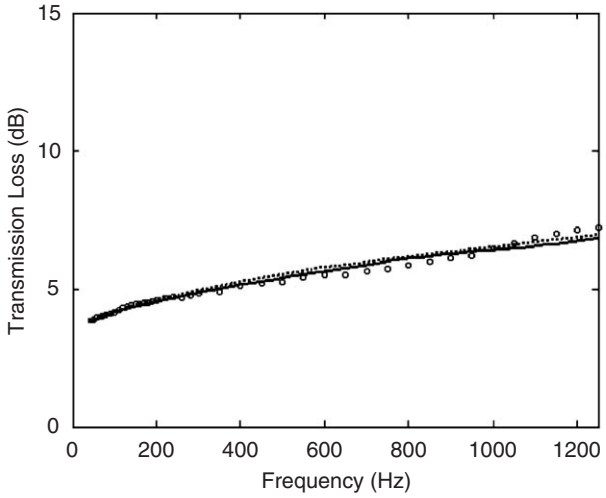

Fig. 13. Measured and predicted transmission loss for the (RC200/12) filter at $M = 0.015$ before the inlet of the filter and $T = 293\,^{\circ}\mathrm{K}$. °°°°, Measured; —, predicted using present theory; …., predicted using the modified 1-D Model.

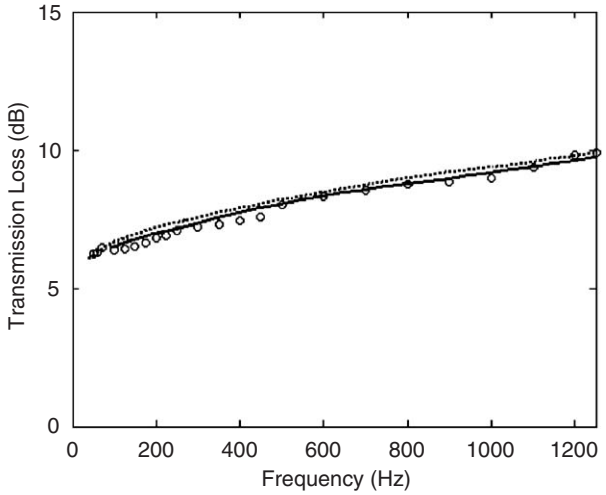

Fig. 14. Measured and predicted transmission loss for the (RC200/20) filter at $M = 0.021$ before the inlet of the filter and $T = 293\,^{\circ}\mathrm{K}$. °°°°, Measured; —, predicted using present theory; …., predicted using the modified 1-D Model.

description of the visco-thermal boundary layers in the quadratic channels. The new model has been validated by comparison with experimental data for clean filters at room temperature. When applied to realistic operating conditions the new model shows that the earlier proposed 1-D model works satisfactorily up to 800–1000 Hz for a typical filter. An improved version of the 1-D model (Section 2.4) using the classical (exact) Kirchhoff solution for a plane wave in a narrow tube is also presented. This modified 1-D model is in close agreement with the predictions of the new model.

At the inlet and the outlet of the filter there are area discontinuities which require the use of acoustic coupling conditions. This question has been studied and the coupling condition suggested in Ref. [11] has been compared to an alternative, based on conservation of energy and momentum. The difference is found to be negligible for typical filters at operating conditions. With the results of this paper and Ref. [11], it seems that good models for the acoustics of DPFs have been found. What remains is to finally validate these models by tests performed at operating conditions. Such tests should preferably be done with the filter connected to a running engine to ensure soot loading. The assumption of a negligible effect on the acoustics of the slow burning of soot that occurs can then be tested.

Acknowledgment

Financial support from the EC-project ARTEMIS (G3RD-CT-2001-00511) is acknowledged.

Appendix A

Multiplying Eq. (8) by $\sin(m'\pi y/2a_j)\sin(n'\pi z/2a_j)$ and integrating over the cross-section yields

$$\sum\nolimits_{m,n} a_{mn}\beta_j^2\alpha_{mn}(\beta_j a_j)I_1 = \left(\frac{\mathrm{i}k_1\Gamma}{\mu_j}\right)I_2, \tag{A.1}$$

where α_{mm} is defined in connection with Eq. (13) and

$$I_1 = \iint_{2a_j\times 2a_j} \sin\left(\frac{m\pi y}{2a_j}\right)\sin\left(\frac{n\pi z}{2a_j}\right)\sin\left(\frac{m'\pi y}{2a_j}\right)\sin\left(\frac{n'\pi z}{2a_j}\right)\mathrm{d}y\,\mathrm{d}z = \begin{cases} a_j^2, m=m', n=n' \\ 0, m\neq m', n\neq n' \end{cases}, \tag{A.2}$$

and

$$I_2 = \iint_{2a_j\times 2a_j} \sin\left(\frac{m'\pi y}{2a_j}\right)\sin\left(\frac{n'\pi z}{2a_j}\right)\mathrm{d}y\,\mathrm{d}z = \frac{16a_j^2}{m'n'\pi^2}, \tag{A.3}$$

where m' and n' are odd integers. Using the results of Eqs. (A.2) and (A.3) in Eq. (A.1) gives the following expression for the Fourier coefficients:

$$a_{mn} = \frac{16\mathrm{i}k_1\Gamma}{\pi^2 mn\mu_j\beta_j^2\alpha_{mn}(\beta_j a_j)}. \tag{A.4}$$

Appendix B

B.1. Acoustic coupling condition at the filter inlet

At the inlet of a diesel particulate filter there is an area contraction, which implies a discontinuity in the acoustic variables and the need for a coupling two-port. This coupling two-port will be derived assuming a quasi-steady model and an incompressible mean flow.

By assuming the conservation of the energy at the area contraction (i.e. no jet formation and no losses) Bernoulli gives for the mean flow

$$P_{\mathrm{IN}} + \tfrac{1}{2}\rho_{\mathrm{IN}} U_0^2 = P_{\mathrm{I}} + \tfrac{1}{2}\rho_{\mathrm{I}} U_{\mathrm{I}}^2, \tag{B.1}$$

where IN denotes the main duct before the DPF inlet and I is the short impermeable narrow pipes after the area contraction as shown in Fig. 1.

Assuming small acoustic perturbations (p and u) gives

$$p_{\mathrm{IN}} + \rho_{\mathrm{IN}} U_{\mathrm{IN}} u_{\mathrm{IN}} = p_{\mathrm{I}} + \rho_{\mathrm{I}} U_{\mathrm{I}} u_{\mathrm{I}}, \tag{B.2}$$

where the steady-state equation has been subtracted out. Similarly the conservation of mass flow implies that

$$\rho_{\mathrm{IN}} A_{\mathrm{IN}} u_{\mathrm{IN}} = \rho_{\mathrm{I}} A_{\mathrm{I}} u_{\mathrm{I}} N, \tag{B.3}$$

where N is the number of open channels. Introducing the fluctuating volume flow $q = Au$ and assuming $\rho_{\mathrm{I}} = \rho_{\mathrm{IN}}$ gives

$$\begin{aligned} p_{\mathrm{IN}} + \rho_{\mathrm{IN}} U_{\mathrm{IN}} q_{\mathrm{IN}}/A_{\mathrm{IN}} &= p_{\mathrm{I}} + \rho_{\mathrm{I}} U_{\mathrm{I}} q_I/A_I, \\ q_{\mathrm{IN}} &= N q_{\mathrm{I}}. \end{aligned} \tag{B.4}$$

By using $U_{\mathrm{I}} = U_{\mathrm{IN}} A_{\mathrm{IN}}/NA_{\mathrm{I}}$, a two-port for the entire DPF inlet can be obtained in two-port matrix form

$$\begin{pmatrix} p_{\mathrm{IN}} \\ q_{\mathrm{IN}} \end{pmatrix} = \begin{pmatrix} 1 & Z_{\mathrm{IN}} M_{\mathrm{IN}} \left((A_{\mathrm{IN}}/NA_{\mathrm{I}})^2 - 1 \right) \\ 0 & 1 \end{pmatrix} \begin{pmatrix} p_{\mathrm{I}} \\ N q_{\mathrm{I}} \end{pmatrix}, \tag{B.5}$$

where $Z_{\mathrm{IN}} = \rho_{\mathrm{IN}} c_{\mathrm{IN}}/A_{\mathrm{IN}}$. This two-port can be written as

$$\mathbf{T} = \begin{pmatrix} 1 & Z_{\mathrm{IN}} M_{\mathrm{IN}} \left(1/m_{\mathrm{IN}}^2 - 1 \right) \\ 0 & 1 \end{pmatrix}, \tag{B.6}$$

where m_{IN} is the open area ratio at the inlet of the DPF.

B.2. Acoustic coupling condition at the filter outlet

Instead of the conservation of energy the momentum equation [14,15] has to be used with the mass flux conservation to calculate the transfer matrix as follows:

$$(P_{\mathrm{III}} - P_{\mathrm{OUT}}) A_{\mathrm{OUT}} = \rho_{\mathrm{OUT}} A_{\mathrm{OUT}} U_{\mathrm{OUT}}^2 - \rho_{\mathrm{III}} N A_{\mathrm{III}} U_{\mathrm{III}}^2. \tag{B.7}$$

Using the same procedure as above to obtain a relationship for small fluctuating quantities and by assuming $\rho_{\mathrm{III}} = \rho_{\mathrm{OUT}}$ gives

$$\begin{aligned} p_{\mathrm{III}} + 2\rho_{\mathrm{III}} U_{\mathrm{III}} q_{\mathrm{III}}/A_{\mathrm{OUT}} &= p_{\mathrm{OUT}} + 2\rho_{\mathrm{OUT}} U_{\mathrm{OUT}} q_{\mathrm{OUT}}/A_{\mathrm{OUT}}, \\ q_{\mathrm{III}} &= q_{\mathrm{OUT}}. \end{aligned} \tag{B.8}$$

By using $U_{III} = U_{OUT}A_{OUT}/NA_{III}$ we get

$$p_{III} = p_{OUT} + 2\rho_{OUT}U_{OUT}q_{OUT}/A_{OUT} - \frac{2\rho_{OUT}U_{OUT}}{NA_{III}}q_{OUT}$$
$$Nq_{III} = q_{OUT} \tag{B.9}$$

which in two-port form becomes

$$\mathbf{T} = \begin{pmatrix} 1 & 2Z_{OUT}M_{OUT}(1 - 1/m_{OUT}) \\ 0 & 1 \end{pmatrix}, \tag{B.10}$$

where $Z_{OUT} = \rho_{OUT}c_{OUT}/A_{OUT}$ and m_{OUT} is the open area ratio at the outlet of the DPF. Note the open area ratio at the inlet is less than the open area ratio at the outlet for a loaded filter.

References

[1] A.D. Pierce, *Acoustics*, Mc Graw-Hill, New York, 1981.
[2] L. Rayleigh, The Theory of Sound, Second ed., vol. 2, Dover, New York, 1945.
[3] K. Peat, A first approximation to the effects of mean flow on sound propagation in capillary tubes, *Journal of Sound and Vibration* 175 (1994) 475–489.
[4] R.J. Astley, A. Cummings, Wave propagation in catalytic converter: formulation of the problem and finite element scheme, *Journal of Sound and vibration* 188 (5) (1995) 635–657.
[5] E. Dokumaci, Sound transmission in narrow pipes with superimposed uniform mean flow and acoustic modelling of automobile catalytic converters, *Journal of Sound and vibration* 182 (1995) 799–808.
[6] J.-G. Ih, C.M. Park, H.-J. Kim, A model for sound propagation in capillary ducts with mean flow, *Journal of Sound and Vibration* 190 (2) (1996) 163–175.
[7] K.-W. Jeong, J.-G. Ih, A numerical study on the propagation of sound through capillary tubes with mean flow, *Journal of Sound and Vibration* 198 (1) (1996) 67–79.
[8] E. Dokumaci, On transmission of sound in circular and rectangular narrow pipes with superimposed mean flow, *Journal of sound and vibration* 210 (3) (1998) 375–389.
[9] E. Dokumaci, An approximate dispersion equation for sound waves in a narrow pipe with ambient gradients, *Journal of Sound and Vibration* 240 (4) (2001) 637–646.
[10] A.G. Konstandopoulos, J.H. Johnson, Wall-flow diesel particulate filters — their pressure drop and collection efficiency, SAE paper No. 890405, 1989.
[11] S. Allam, M. Åbom, Acoustic modelling and testing of diesel particulate filters, *Journal of Sound and Vibration* 288 (1/2) (2005) 255–273.
[12] D.H. Keefe, Acoustical wave propagation in cylindrical ducts: transmission line parameter approximations for isothermal and nonisothermal boundary conditions, *Journal of the Acoustical Society of America* 75 (1) (1984) 58–62.
[13] M.L. Munjal, *Acoustics of Ducts and Mufflers*, John Wiley, New York, 1987.
[14] D. Ronneberger, Experimentelle Untersuchungen Zum akustischen Reflexionsfaktor Von Unstetigen Uuerschnittsänderungen in Einem Luftdurchströmten Rohr, *Acustica* 19 (1967) 222–235.
[15] P.O.A.L. Davies, Practical flow duct acoustics, *Journal of Sound and Vibration* 124 (1988) 91–115.